GEOPHYSICS, VOL. 73, NO. 5 (SEPTEMBER-OCTOBER 2008); P. Q29–Q42, 29 FIGS., 1 TABLE.
10.1190/1.2969058

The spatial data-adaptive minimum-variance distortionless-response beamformer on seismic single-sensor data

Ionelia Panea[1] and Guy Drijkoningen[2]

ABSTRACT

Coherent noise generated by surface waves or ground roll within a heterogeneous near surface is a major problem in land seismic data. Array forming based on single-sensor recordings might reduce such noise more robustly than conventional hardwired arrays. We use the minimum-variance distortionless-response (MVDR) beamformer to remove (aliased) surface-wave energy from single-sensor data. This beamformer is data adaptive and robust when the presumed and actual desired signals are mismatched. We compute the intertrace covariance for the desired signal, and then for the total signal (desired signal + noise) to obtain optimal weights. We use the raw data of only one array for the covariance of the total signal, and the wavenumber-filtered version of a full seismic single-sensor record for the covariance of the desired signal. In the determination of optimal weights, a parameter that controls the robustness of the beamformer against an arbitrary desired signal mismatch has to be chosen so that the results are optimal. This is similar to stabilization in deconvolution problems. This parameter needs to be smaller than the largest eigenvalue provided by the singular value decomposition of the presumed desired signal covariance. We compare results of MVDR beamforming with standard array forming on single-sensor synthetic and field seismic data. We apply 2D and 3D beamforming and show prestack and poststack results. MVDR beamformers are superior to conventional hardwired arrays for all examples.

INTRODUCTION

In recent years, the number of seismic acquisition channels has increased dramatically, which has led geophysicists to question the use of hardwired arrays. Conventionally, seismic arrays were needed to reduce certain types of noise. This reduction then placed some requirements on the data, the most important being that reflections, seen as the desired signal, should not be aliased spatially. The most difficult seismic arrival on the land data is ground roll, which requires much finer spatial sampling than reflections. Therefore, the array should work as a spatial antialias and resampling operator (Vermeer, 1990). However, with modern high channel counts, fast data transfer, and storage, the array should no longer be considered hardwire connected, but as a digital array that can be treated by more sophisticated digital processing.

Digital array processing is being used in many fields. A common denominator for this is the so-called beamformer, which is a processor applied to data from an assembly of sensors to increase the signal-to-noise ratio. It belongs to a class of spatial filters applied when signals and noise overlap in frequency content but arrive from different spatial directions (Van Veen and Buckley, 1988; Van Veen, 1991). In a beamformer, weights are applied to single array elements to create a beam. Generally, beamformers can be data independent, statistically optimum, data adaptive, or partially data adaptive, depending on the procedure for determining weights (Van Veen and Buckley, 1988).

In the case of data-independent beamformers, weights are fixed to be independent of the received data. For statistically optimum equipment, weights are based on statistics of the data recorded by the array. Statistics usually are not known and might change over time, so adaptive algorithms are required. The data-adaptive beamformer is designed so the response is optimal with respect to the data themselves. Partially data-adaptive beamformers are designed to reduce the computational load and associated cost of the data-adaptive algorithms.

It has been demonstrated that, under ideal conditions, data-adaptive beamformers achieve a better signal-to-noise ratio in comparison with conventional ones (Feldman and Griffiths, 1994). It also was shown that the response of data-adaptive beamformers is sensitive to mismatch between the presumed and actual array response. An example of possible mismatch and a solution for dealing with it is given in Shahbazpanahi et al. (2003). In addition, the quality of a da-

Manuscript received by the Editor 12 April 2007; revised manuscript received 18 April 2008; published online 17 September 2008.
[1]University of Bucharest, Faculty of Geology and Geophysics, Bucharest, Romania. E-mail: lili@gg.unibuc.ro; ipanea2@yahoo.com.
[2]Delft University of Technology, Department of Geotechnology, Delft, The Netherlands. E-mail: g.g.drijkoningen@tudelft.nl.

ta-adaptive beamformer depends on the number of analyzed samples used in the data covariance matrix.

Different types of data-adaptive beamformers have been proposed during the last two decades. For the specific case of mismatch between the presumed and actual signal-look directions, algorithms such as the linearly constrained minimum-variance beamformer (see Johnson and Dudgeon, 1993), signal-blocking-based algorithms (Godara, 1986), and Bayesian beamformer (Bell et al., 2000) have been developed. Another approach in the presence of unknown arbitrary-type mismatch of the desired signal array response is proposed in the minimum-variance distortionless-response (MVDR) beamformer (Monzingo and Miller, 1980; Jian et al., 2003; Vorobyov et al., 2003). An analysis of the performance of the MVDR in the context of errors in signal-look direction is made by Wax and Anu (1996).

Characteristics of the MVDR beamformer make it suitable for use with seismic data because it is computed based on raw single-sensor seismic data containing the desired signal and noise. Its purpose is to calculate weights to be applied for each group of single-element recordings before their summation. These weights will differ between groups because of their individual data covariance matrices in the weight-definition formula. In this way, we define a proper data-adaptive beamformer.

Design of an MVDR beamformer

In this section, we describe briefly the adaptive MVDR beamformer, based on the demonstration from Shahbazpanahi et al. (2003). In addition, we emphasize differences required by its application on the single-sensor seismic data. Its definition is based on the knowledge of two types of records, one with noise and the other with a desired signal. In seismic exploration, the desired signal is defined as the primary reflected energy. Noise is defined as anything except primary reflected energy, such as multiply reflected and refracted waves, diffractions, and surface waves.

Surface waves, also known as ground roll, are very important in land seismic data. They are difficult to attenuate because their frequency content overlaps with that of reflected waves. Furthermore, surface waves can be affected strongly by spatial aliasing because the correct receiver spacing, to allow for an optimum recording of the reflected waves, is too large for the ground roll. A traditional effective way to attenuate the surface-wave signal is to use an appropriate receiver array (Anstey, 1986). The spacing between array elements is arranged so that surface waves are not aliased within the array. The size of the group interval (spacing between arrays) is chosen so that reflected waves are not aliased spatially.

A beamformer can be designed to compute weights based on single-element recordings and apply the weights to individual recordings before summing them into the beam.

First, let us assume receiver responses at time t are defined as

$$\mathbf{x}(t) = \mathbf{s}(t) + \mathbf{n}(t), \tag{1}$$

where $\mathbf{x}(t)$ is the vector of single-element observations, $\mathbf{s}(t)$ is the desired signal vector, and $\mathbf{n}(t)$ is the noise vector. Therefore, over the entire analyzed time interval, the data $\mathbf{x}$ are given by the signal $\mathbf{s}$ and noise $\mathbf{n}$ part. In the case of synthetic or field seismic records, these two parts can be determined by modeling or using simple preprocessing algorithms. The signal-to-noise ratio, denoted by S/N, can be defined by using the statistical expectation of the desired signal and noise, which gives us the signal covariance denoted by $\mathbf{R}_s$ and noise denoted by $\mathbf{R}_n$. When applying weights, S/N can be written as follows:

$$\mathrm{S/N} = \frac{\mathbf{w}^T\mathbf{R}_s\mathbf{w}}{\mathbf{w}^T\mathbf{R}_n\mathbf{w}}, \tag{2}$$

where $\mathbf{w} = [w_1, w_2, \ldots, w_M]^T$, a weight vector to be determined, based on an array with M elements. In this expression, covariances $\mathbf{R}_s$ and $\mathbf{R}_n$ are positive semidefinite matrices of size $M \times M$.

Next, Shahbazpanahi et al. (2003) select a weight vector $\mathbf{w}$ so that S/N is maximized. Above all, the desired signal must be protected. This is guaranteed by requiring that $\mathbf{w}^T\mathbf{R}_s\mathbf{w} = 1$, which means there is no signal cancellation (Shahbazpanahi et al., 2003). Maximizing S/N is equal to minimizing noise, so weights for a maximal S/N are obtained from the following minimization equation:

$$\min_{\mathbf{w}} \mathbf{w}^T\mathbf{R}_n\mathbf{w} \text{ subject to } \mathbf{w}^T\mathbf{R}_s\mathbf{w} = 1. \tag{3}$$

This defines the general type of minimum-variance distortionless-response (MVDR) beamformer. Note that this type of beamformer requires separation of the desired signal and noise as expressed by matrices $\mathbf{R}_s$ and $\mathbf{R}_n$, related to equation 1. This MVDR beamformer was proposed by Capon (1969), and more data-adaptive versions were proposed and studied in the following years (see Zoltowski, 1988; Van Veen, 1991; Raghunath and Reddy, 1992; Harmanci et al., 2000). The high resolution, low sidelobes, and good interference suppression are examples of properties of the MVDR beamformer.

Following Shahbazpanahi et al. (2003) and Voroboyov et al. (2003), the solution to the minimization problem in equation 3 might be found using the Lagrange-multipliers method. The optimal weight vector is obtained as

$$\mathbf{w}_{opt} = P\{\mathbf{R}_n^{-1}\mathbf{R}_s\}, \tag{4}$$

where $P\{\cdot\}$ is the operator that yields the principal eigenvector of a matrix, i.e., that corresponds to the maximal eigenvalue. Thereafter, the following output, y (t), is obtained:

$$y(t) = \mathbf{w}_{opt}^T\mathbf{x}(t), \tag{5}$$

which is the MVDR beamformer.

This MVDR beamformer is difficult to apply to seismic data because a seismic recording contains signal and noise. Separate records for these components can be derived via processing techniques or seismic modeling, but their accuracy is limited, and we know from previous studies that the effectiveness of adaptive beamforming algorithms is affected by the presence of errors in the signal and noise covariances (Shahbazpanahi et al., 2003; Vorobyov et al., 2003).

To avoid using records only with noise to determine the noise covariance, it is desirable for seismic purposes to find another definition of the MVDR beamformer that involves the entire data set, meaning records that contain signal and noise. Assuming that the total signal is predominantly surface-wave energy, Reed et al. (1974) propose to replace $\mathbf{R}_n$ with $\mathbf{R}_x$. The data covariance matrix, $\mathbf{R}_x$, is computed based on the raw single-sensor seismic records with signal and noise:

$$\mathbf{R_x} = \frac{1}{N}\mathbf{X}\mathbf{X}^T, \tag{6}$$

where $\mathbf{X}$ is an $M \times N$ data matrix, M is the number of array elements, and N is the number of time samples.

For each time sample, we compute the intertrace covariance for the desired signal and then the total signal. Equation 4 then can be written as

$$\mathbf{w}_{opt} = P\{\mathbf{R_n}^{-1}\mathbf{R_s}\} \cong P\{\mathbf{R_x}^{-1}\mathbf{R_s}\}. \tag{7}$$

This replacement was necessary because, in practical situations, the noise (with or without interference) covariance matrix is unavailable. It s shown that if the signal component is present in the training data, this replacement decreases the performance of the beamformer, whose weights are determined using equation 7 (Reed et al., 1974; Shahbazpanahi et al., 2003; Vorobyov et al., 2003). Therefore, other algorithms that define more robust adaptive beamformers were proposed. For example, algorithms are developed in the presence of arbitrary unknown steering vector mismatches (Vorobyov et al., 2003) or in the presence of mismatches between the presumed and actual desired response (Shahbazpanahi et al., 2003).

Based on equation 7, optimal weights are computed using the entire data. Still, one disadvantage is introduced through the use of the signal covariance matrix, $\mathbf{R_s}$, because it is a source of error that can degrade the quality of the MVDR beamforming response. To prevent this, Shabazpanahi et al. (2003) introduce an error matrix, $\mathbf{\Delta}$, in the definition of the signal covariance matrix so that it represents the possible mismatch between the presumed, $\mathbf{R_s}$, and actual, $\acute{\mathbf{R}}_\mathbf{s}$, signal covariance matrices:

$$\mathbf{R_s} = \acute{\mathbf{R}}_\mathbf{s} + \mathbf{\Delta}, \tag{8}$$

where $\mathbf{\Delta}$ is an $M \times M$ unknown, positive, semidefinite error matrix whose norm is bounded by a known constant $\varepsilon > 0$. Shahbazpanahi et al. (2003) include this error matrix in the constraint equation from the MVDR beamformer definition:

$$\min_{\mathbf{w}} \mathbf{w}^T\mathbf{R_x}\mathbf{w} \text{ subject to } \mathbf{w}^T(\mathbf{R_s} + \mathbf{\Delta})\mathbf{w} \geq 1 \text{ for all } \|\Delta\| \leq \varepsilon. \tag{9}$$

The weight vector, $\mathbf{w}$, and error matrix, $\mathbf{\Delta}$, are unknowns in this definition. The Lagrange-multipliers method is used twice. First, it is used to determine the error matrix and then to solve for the optimal weight vector. The detailed mathematical demonstration is given in Shahbazpanahi et al. (2003). This results in optimal weights

$$\mathbf{w}_{opt} = P\{\mathbf{R_x}^{-1}(\mathbf{R_s} - \varepsilon\mathbf{I})\}, \tag{10}$$

which is the robust form of the MVDR beamformer.

The optimal value of ε is determined by the analysis of eigenvalues obtained after the singular value decomposition of the presumed desired signal covariance matrix (Shahbazpanahi et al., 2003). When we deal with synthetic or field single-sensor data, this covariance matrix is computed using the wavenumber-filtered data according to the value of the desired number of array elements. Practically, the optimal value of ε needs to be smaller than the maximum eigenvalue.

The design of the MVDR beamformer for areal array data (3D) is generally the same as for linear array data (2D). The main difference between the designs is the size of the input data being a function of the number of receivers. In the 2D case, the input data are vectors of size M and for the 3D case MP, where M is the number of inline and P the number of crossline single sensors. Because the size of input vectors is larger, the size of the signal and data covariance matrices is greater, namely $MP \times MP$. The derivation is the same as for the 2D case, only vectors now contain areal instead of linear array data. Then the result is precisely as expressed in equation 10 where the weight vector now has the size MP.

MVDR beamformers on synthetic seismic data

In this section, we show the application of the 2D and 3D MVDR beamformer-to-synthetic data obtained by seismic modeling. This was done using two modeling approaches, one by simply creating a constant-amplitude linear and hyperbolic event, and the other by the finite-difference method. MVDR results are compared with a standard array response whose weights are fixed and equal to one. The modeling with the linear and hyperbolic events was made in the presence of phase and amplitude variations, but the first example presented omits these.

2D modeling with no amplitude/phase variations

We first considered a response containing a linear and a hyperbolic event as shown in Figure 1. The linear event is characterized by slow apparent velocity (440 m/s) and low frequency (16 Hz). It can be considered a surface wave that is seen as noise to be attenuated. The hyperbolic event is characterized by high apparent velocity and frequency (36 Hz), representing a reflected wave considered a desired signal to be protected. The depth of the reflector is 300 m. We used a Ricker wavelet. The first response to consider was 12 traces coming from 12 single sensors spaced 5 m.

In seismic practice, an array consists of hardwired connected receivers, so simulation is achieved by summing individual recordings as one output. This is the first step in array forming (Hoffe et al., 2002). The second step is spatial resampling to a desired spacing. For the MVDR beamformer, we used optimal weights determined from equation 10, the data covariance matrix $\mathbf{R_x}$ of the data based on 12 input traces, and the signal covariance matrix $\mathbf{R_s}$ of the desired signal from 12 input traces containing only the reflected wave. Parameter ε was determined by testing different values smaller than the maximum eigenvalue provided by the singular value decomposition

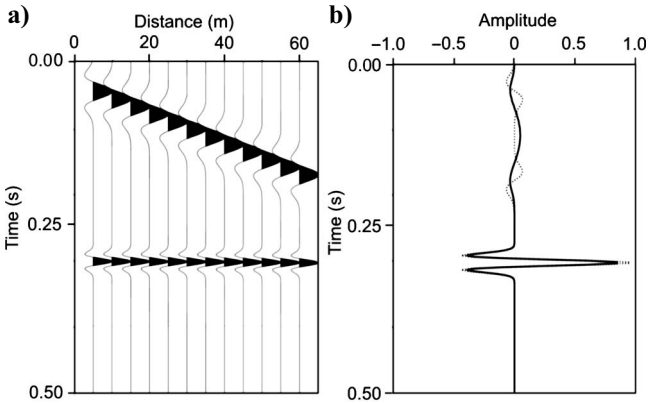

Figure 1. (a) Synthetic seismogram with 12 traces after (b) standard array forming (dashed line) and MVDR beamforming (solid line).

of the signal covariance matrix. The optimal value of ε is one for which the error e_{tx}, computed using equation 11, is minimum (see Figure 2);

$$e_{tx} = \frac{1}{N_t} \sum_{n=1}^{N_t} |y_n^d - y_n^s|, \tag{11}$$

where e_{tx} is the error in amplitude computed in the time domain, y^d is the desired response, y^s is the standard array forming or MVDR beamforming response, and N_t is the total number of time samples. For this record, the optimal value of ε is 0.001.

When comparing results shown in Figure 1, one notices that the MVDR beamformer attenuates surface waves better than standard array forming. However, additional analysis shows the reflected signal is better preserved after standard array forming (see Figure 1). In addition, the remaining noise seen on the MVDR beamforming response is characterized by a lower frequency 4–6 Hz response than that seen on the standard array forming response of about 12 Hz. The error in amplitude for different ε values and MVDR weights computed for the chosen ε value are displayed in Figure 2.

The noise attenuation by standard array forming or MVDR beamforming can be quantified by using equation 11. For the example, the error e_{tx} for the standard array forming response is $2.39 \cdot 10^{-4}$, and for the MVDR beamforming response it is $2.03 \cdot 10^{-4}$. The smaller error obtained for the MVDR response means that it is closer to the desired array response.

To look at spatial characteristics, we created a larger set of single-sensor recordings in which multiple arrays are formed (see Figure 3). The same modeling parameters as before are used for frequencies, velocities, and single-sensor spacing. The depth of the reflector is 400 m. We used 80 single sensors and applied the MVDR and standard array-forming processing to compare the attenuation effectiveness of the slow linear event. Because the goal of array forming is to spatially filter and subsample the data, the whole surface-wave signal does not need to be removed, but only the part that will be outside the new spatial band (wavenumbers that are not aliased after subsampling). As we show later, there are situations when standard array forming does not attenuate adequately out-of-the-new-spatial-band energy, which means that part of the surface waves will be aliased spatially after resampling to a larger group interval. Attenuation is better achieved using the MVDR adaptive beamformer. Because the reflected wave is characterized by a small moveout, MVDR could preserve the frequency content of it. In the case of reflected waves with large moveout, the wavelet is stretched after the

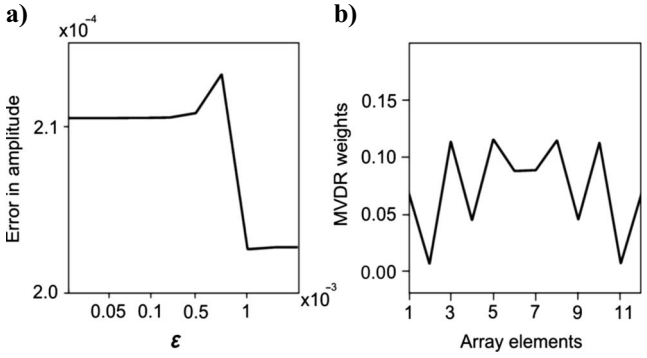

Figure 2. (a) Different ε values used in analysis and (b) MVDR beamformer weights computed for the optimal $\varepsilon = 0.001$.

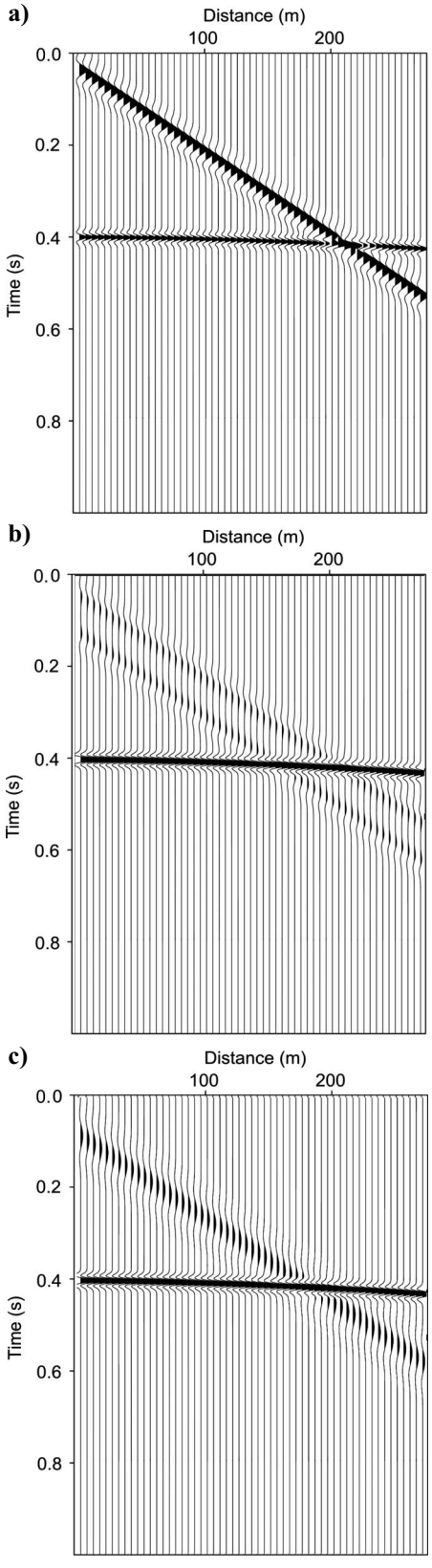

Figure 3. (a) Windowed synthetic seismogram in distance after (b) standard array forming and (c) MVDR beamforming, displayed in the time domain.

summing of weighted traces. Therefore, the frequency is lower. In these situations, we perform time corrections and reflected waves are protected (Panea and Drijkoningen, 2006).

We applied MVDR to this record to attenuate out-of-the-new-spatial-band surface waves. This algorithm was applied to an array of 12 elements. A flowchart of the application of the MVDR beamformer algorithm is shown in Figure 4.

The computation of data and signal covariance matrices was done for a sliding window of 12 traces as 1–12, 2–13, 3–14, etc. (traces that need to be summed after we apply optimal weights). The intertrace covariance for the desired signal was computed using groups of traces chosen from a k-filtered single-sensor record that contains only the band energy determined for the group interval of 10 m. Based on the singular value decomposition of the signal covariance matrix, we obtain a set of eigenvalues (see Figure 5a in which we display eigenvalues determined for traces 10–21). After the analysis of errors in amplitude computed for different ε values, the value of 0.0005 was chosen as optimal (see Figure 5b). The ε value is smaller than the maximum eigenvalue obtained for each group of elementary recordings. Then for this ε value, we computed MVDR beamformer weights (see Figure 5c).

The error in amplitude e_{fk} is computed using:

$$e_{fk} = \frac{1}{N_f}\frac{1}{N_k}\left(\sum_{f=1}^{N_f}\sum_{k=-N_{k\_old}}^{-N_{k\_new}} |\tilde{y}^s_{f,k} - \tilde{y}^d_{f,k}| + \sum_{f=1}^{N_f}\sum_{k=+N_{k\_new}}^{+N_{k\_old}} |\tilde{y}^s_{f,k} - \tilde{y}^d_{f,k}|\right), \quad (12)$$

where e_{fk} is the error, $\tilde{y}^d$ is the (f, k_x)-domain amplitude spectrum of the desired response, which should be zero on these two wavenumber intervals; $\tilde{y}^s$ is the (f, k_x)-domain amplitude spectrum of the standard array forming or MVDR beamforming response; N_k is the wavenumber sample quantity; and N_f is the number of frequency samples.

The response of a standard array also was computed (see Figure 3b). We display only the output of the first step of array forming, namely adding traces. The second step is represented by spatial resampling to a group interval that will not alias spatially the reflected waves. The first step is more important than the subsequent spatial resampling because it gives us a spatially broadband picture of the noise attenuation.

By comparing responses of these two algorithms, we see that the MVDR beamforming achieved better out-of-the-new-spatial-band attenuation than standard array forming. The remaining noise seen on the MVDR beamforming response is characterized by a very low frequency of about 4–6 Hz compared with the original of 16 Hz. In contrast, the standard array forming response contains two clear linear events with the same slowness as the original one, but arriving with only slightly lower frequencies than initially, at about 12 Hz.

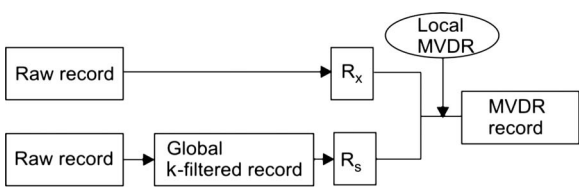

Figure 4. Flow diagram for MVDR beamforming.

The (f, k_x)-domain amplitude spectrum of the initial record before array forming is shown in Figure 6a and after the wavenumber filtering is shown in Figure 6b. It can be observed that neither arrival is affected by extra spatial aliasing as a result of spatial subsampling. We also notice that if we spatially resample both responses to a group interval of 10 m giving a Nyquist wavenumber of 0.05 m^{-1}, the remaining surface wave on the standard array forming response would be more spatially aliased compared with the MVDR beamforming response.

The attenuation of the slow linear event can be quantified by defining the difference between the out-of-the-new-spatial-band energy in the (f, k_x)-domain of the desired response and of the standard array forming or MVDR beamforming response (see equation 12). The desired response is considered to be a record with all energy above the new Nyquist wavenumber zero. A value of 0.0058 was obtained for e_{fk} in the case of standard array forming and 0.0052 for MVDR beamforming. Based on these values, we obtained better noise attenuation with MVDR beamforming.

2D modeling with amplitude/phase variations

The synthetic seismogram analyzed above was modeled without phase or amplitude variations. Modeling parameters were chosen to avoid the strong spatial aliasing for both events. Because field seismic records are affected usually by phase and amplitude variation, it is necessary to consider their effect on the MVDR beamforming response. Phase variations can occur because of irregular receiver positioning, variable intra-array static effects, and a large lateral variation of velocity inside the receiver array. Amplitude variations can occur, for example, as a result of imperfection of the geophone ground coupling.

We considered phase variation in modeling the synthetic record. Timing errors were introduced by mispositioning all receivers. We again used the linear and hyperbolic event using 80 irregularly spaced single sensors. A maximum variation of 20% within the re-

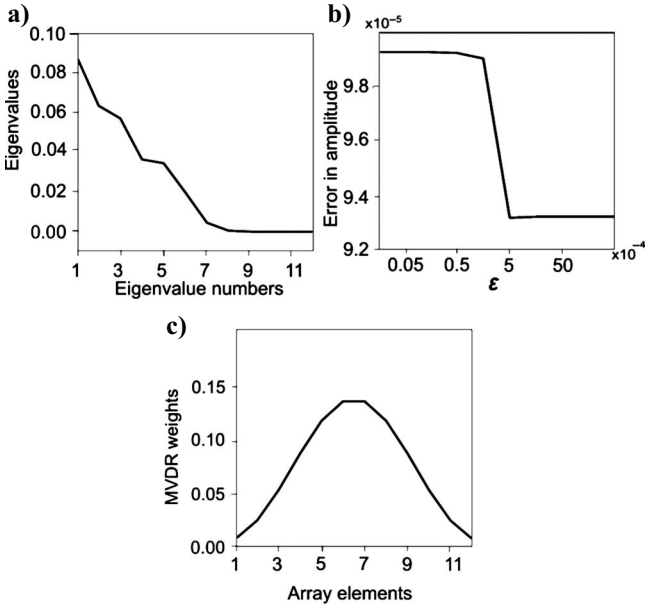

Figure 5. (a) Eigenvalues obtained after the singular value decomposition of $\mathbf{R}_s$, (b) error in amplitude computed for different ε values and (c) MVDR weights computed for the optimal $\varepsilon = 0.0005$.

ceiver spacing of 5 m was allowed. The seismogram is displayed in Figure 7a and its (f, k_x)-domain amplitude spectrum is shown in Figure 8a. The effect of the phase variation is clear on the (t, x)- and (f, k_x)-domain panels. The variation generated some aliased energy seen on the (f, k_x)-domain amplitude spectrum, observable as inclined stripes.

Next, we applied standard array and MVDR beamforming assuming an array of 12 elements. Results are shown in Figure 7b and c. Again, computation of the data and signal covariance matrices was done for windows of traces 1–12, 2–13, 3–14, etc. Traces used for the $\mathbf{R}_s$ computation have been chosen from a globally k-filtered record that contains only the new-spatial-band energy determined for the desired group interval of 10 m. The optimal ε value of 0.0004 was determined for the smallest error in amplitude e_{fk}, being smaller than the maximum eigenvalue obtained for each analyzed window of traces. In observing responses for the (t, x)-domain, we noticed good noise attenuation for the standard array-forming response, but greater attenuation to the MVDR beamforming result. The undesired striping energy of the (f, k_x)-domain is well attenuated by standard array forming and MVDR beamforming (see Figure 8b and c). Good results obtained by MVDR beamforming are supported by the quantification of the error e_{fk}, determined by equation 12 as equal to 0.0052 for the MVDR beamforming response. For the standard array, this error is 0.0055.

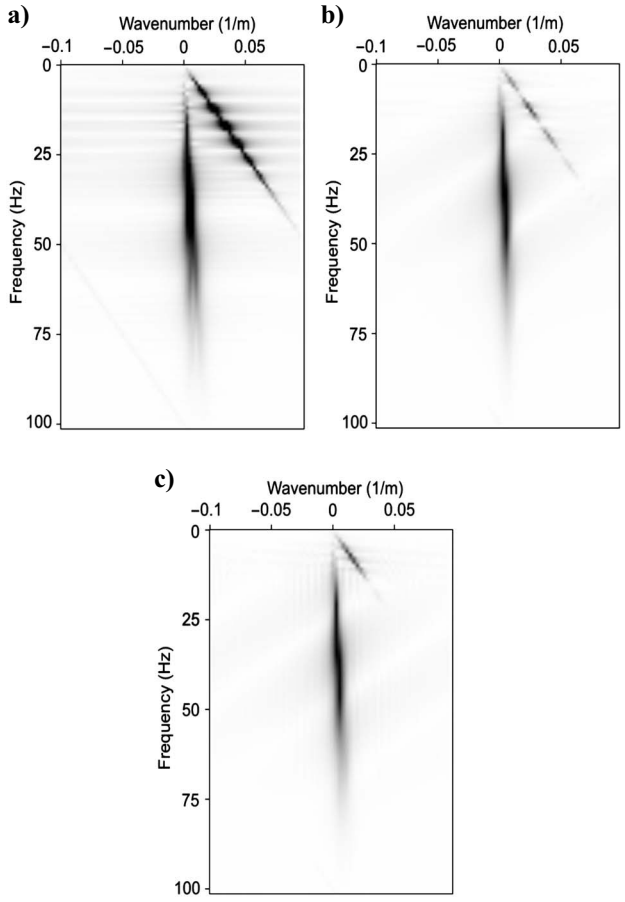

Figure 6. The (f, k_x)-amplitude spectrum of (a) raw synthetic seismogram after (b) wavenumber filtering, (c) standard array forming, and (d) MVDR beamforming. The same display parameters apply.

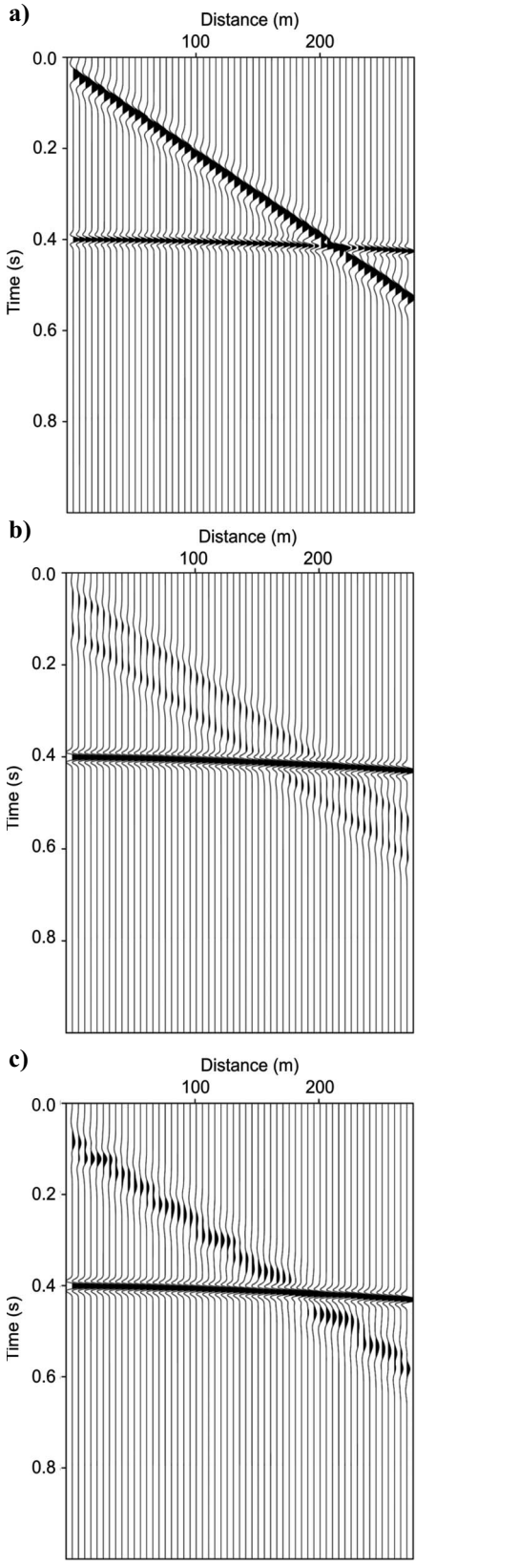

Figure 7. (a) Windowed synthetic seismogram in distance with irregular single-sensor spacing, maximum error 20% of 5 m after (b) standard array forming and (c) MVDR beamforming, displayed in the time domain.

The effect of amplitude variation was analyzed working with synthetic records, and we found that the effect is less than that observed on records with phase variation. The aliased energy generated by this type of variation is well attenuated by the MVDR beamformer (Panea et al., 2005; Panea and Drijkoningen, 2006).

2D finite-difference modeling

So far we have shown the better performance of MVDR compared with standard array forming when considering the simple response of a linear and hyperbolic event. To increase the complexity of records, but still have some control over the outcome, we created synthetic records using the finite-difference method based on the elastic wave equation. The 2D depth model has four horizontal layers with the density and P- and S-wave velocities varying with depth. These parameters are constant along the profile (see Figure 9). A model shot record is displayed in Figure 10. Reflected waves are covered by dispersive surface waves at small offsets, and head waves are abundant at large offsets. Head waves are not well attenuated by array forming because of their high apparent velocity and frequency, which are comparable with reflections. This seismogram is a single-sensor record used as input data to the MVDR beamformer and a standard array.

To prevent spatial aliasing of reflected waves, an array of 12 elements, meaning an array length of 30 m, was used in this case. For the chosen array length, the standard array forming response did not show good noise attenuation. Therefore, we expected the MVDR beamformer would show better out-of-the-new-spatial-band sur-

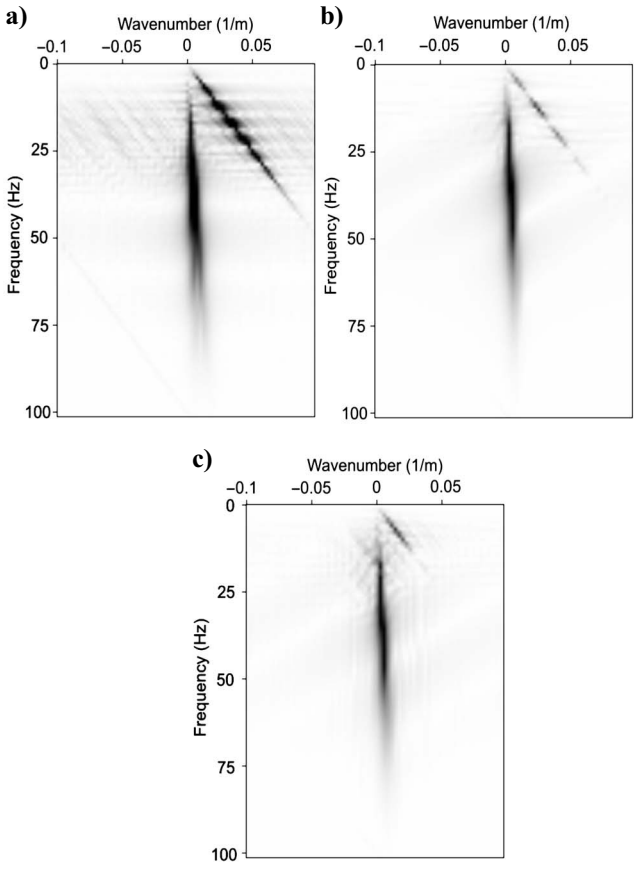

Figure 8. The (f, k_x)-amplitude spectrum of (a) raw synthetic seismogram with irregular single-sensor spacing, maximum error 20 % of 5 m after (b) standard array forming and (c) MVDR beamforming. The same display parameters apply.

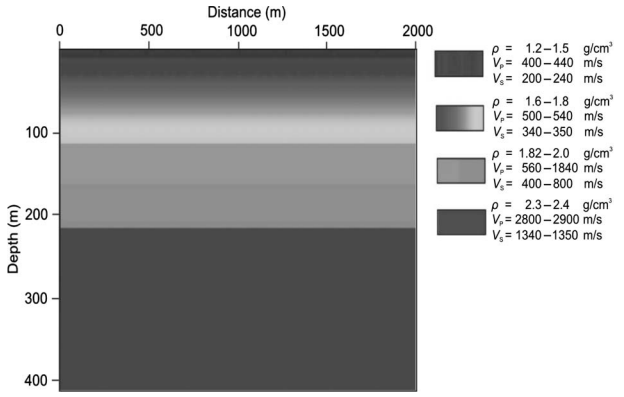

Figure 9. Depth model used for elastic finite-difference modeling; ρ is density, V_p is the P-wave velocity, and V_s is the S-wave velocity.

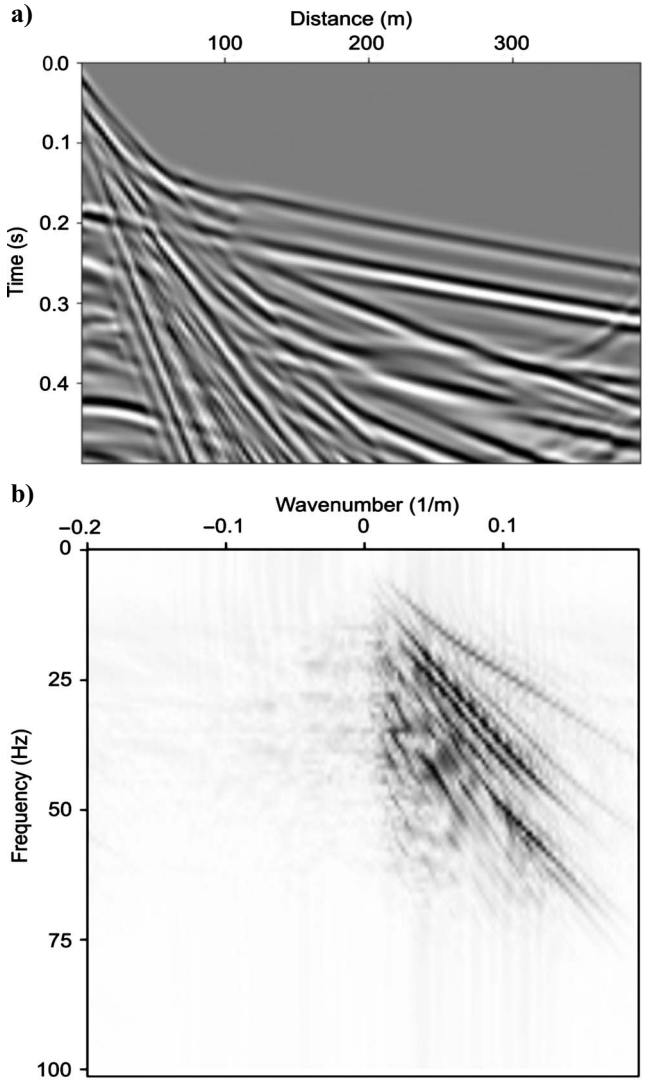

Figure 10. (a) Synthetic seismogram and (b) its (f, k_x)-amplitude spectrum. Modeling parameters: 160 single sensors with 2.5-m spacing, time sampling interval is 1 ms.

face-wave attenuation. For an accurate comparison, we used the same 30-m array length. The application of this algorithm required knowledge of the data covariance matrix, $\mathbf{R}_x$, and the signal covariance matrix, $\mathbf{R}_s$. For $\mathbf{R}_x$, a group of 12 raw traces was used, so $\mathbf{R}_x$ is always a local covariance. For the signal covariance, a full single-sensor record was filtered to eliminate the out-of-the-new-spatial-band energy. Then these k-filtered data were used for the matrix $\mathbf{R}_s$ for all groups of 12 elementary recordings 1–12, 2–13, 3–14, etc., given by individual sensors. In this way, the globally filtered record was used for the computation of all local beamformers in that record.

The matrix $\mathbf{R}_s$ was used for the computation of parameter ε, via singular value decomposition. Optimal beamformer weights were computed for a value of ε smaller than maximum eigenvalues obtained after singular value decomposition. Then optimal weights were computed for each group of single-sensor recordings.

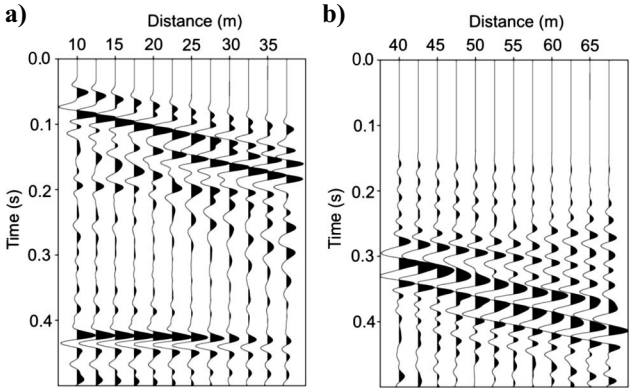

Figure 11. Group of traces located between (a) 10–37.5 m and (b) 40–67.5 m, chosen from the synthetic record displayed in Figure 10a.

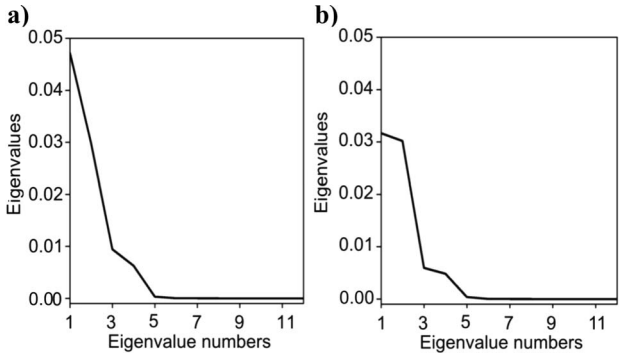

Figure 12. Eigenvalues for the group of traces located between (a) 10–37.5 m and (b) 40–67.5 m.

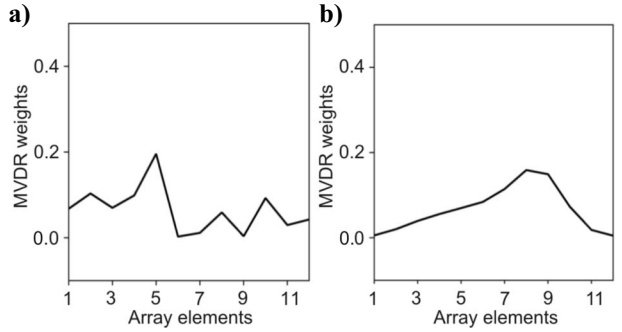

Figure 13. MVDR beamformer weights for the group of traces located between (a) 10–37.5 m and (b) 40–67.5 m.

In Figure 11, we display two groups of 12 single-sensor recordings, chosen from the record displayed in Figure 10a, which were involved in the computation of the standard-array and MVDR beamformer responses. The first one contains traces from the distance interval 10–37.5 m and reflections are clear (see Figure 11a). The second one contains traces from the distance interval 40–67.5 m in which the noise is dominant (see Figure 11b). Using these two raw records as input, we obtain the data covariance matrices. The same windows of traces were chosen from the globally k-filtered record to compute the matrix $\mathbf{R}_s$. This matrix is necessary to compute eigenvalues required by the computation of MVDR beamformer weights (see Figure 12). We display eigenvalues determined for the group of traces placed at small (Figure 12a) and large (Figure 12b) distances from the shot point.

Based on the analysis of these sets of eigenvalues, the ε optimal value chosen was 0.0001. Next, MVDR beamformer weights were calculated and applied to groups of traces before their summation (see Figure 13). Looking at the MVDR beamforming response displayed in Figure 14b, we note appreciable attenuation of out-of-the-new-spatial-band surface waves with clear reflected waves at larger offsets than in the initial record (see Figure 10a). As expected, refracted waves are still high in amplitude, but the same result is seen

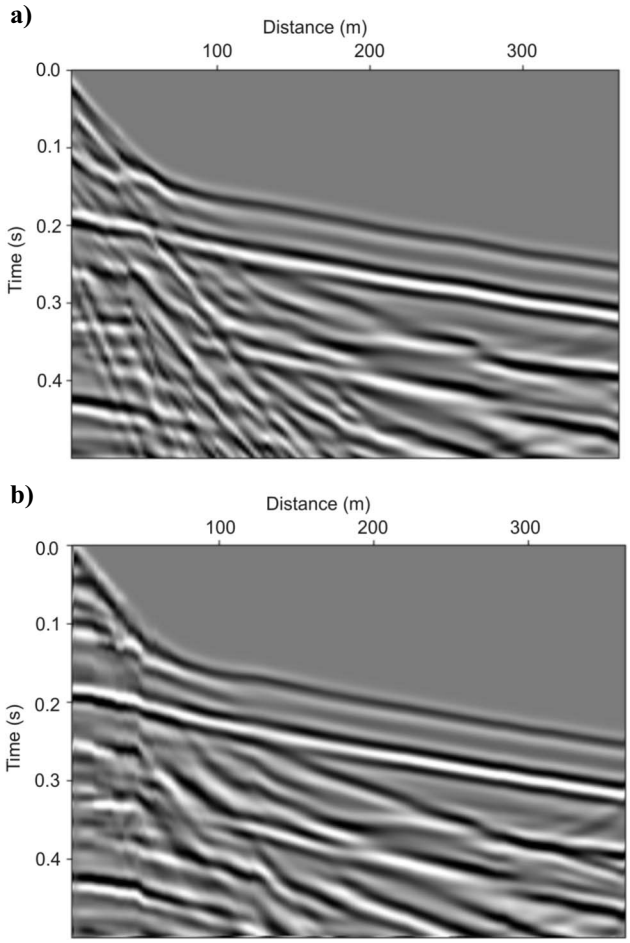

Figure 14. (a) Standard array-forming and (b) MVDR beamforming responses.

for the standard array forming response. Significantly, out-of-the-new-spatial-band surface waves are not attenuated greatly after standard array forming (see Figure 14a). Furthermore, when considering the (f, k_x)-domain representation as shown in Figure 15, the MVDR result contains less energy above 0.05 m^{-1} (compare Figure 15a and b).

If we attempted the second step of spatial resampling, for example to a group interval of 10 m, meaning a Nyquist wavenumber of 0.05 m^{-1}, the remaining surface waves would be aliased spatially in the standard array case and much less so for MVDR. Because the (f, k_x)-domain amplitude spectrum of the MVDR beamformer shows better out-of-the-new-spatial-band attenuation, its spatial resampling would give a record with surface waves scarcely spatially aliased. As a quantification of noise-attenuation efficacy by the MVDR beamformer, error e_{fk} based on equation 12 is 0.0052 for the standard-array response and 0.0028 for the MVDR beamforming response, so the MVDR result is better.

3D finite-difference modeling

In the previous account, we analyzed the effect of the MVDR beamformer on 2D synthetic seismic data. We noticed that surface waves were well attenuated, even in the presence of phase and amplitude variation. Considering that we wish to analyze a partial 3D field data set, we must look at the effect of the 3D MVDR beamformer on 3D synthetic data. We modeled a synthetic data set using the elastic finite-difference code (see Figure 16). The 3D depth model used is an extension of the 2D model shown in Figure 9.

The synthetic record was modeled using a strip of five lines of single sensors spaced at 5 m in inline and crossline directions. The seismic source was located on the third line. The array with six inline and five crossline elements was chosen to prevent the spatial aliasing of arrivals contained by the modeled record (see Figure 17). The group interval was 10 m. MVDR beamformer weights were computed using $\varepsilon = 0.01$. The desired signal is a record showing zero out-of-the-new-spatial-band energy. Consequently, we k-filtered all traces in the global record. The covariance matrix of the desired signal involved in the weight definition then is the presumed signal covariance matrix. The actual signal covariance matrix of the local array was slightly different, but our MVDR takes this into account. The data covariance matrix was computed using the synthetic record that contains desired signal and noise. Consequently, we used only raw traces that belong to the local array.

Looking at the MVDR beamforming response displayed in the (t, x)- and (f, k_x)-domains in Figures 18 and 19, we notice a greater out-of-the-new-spatial-band energy attenuation for the MVDR compared with the result for standard array forming. Remaining surface waves are clear on the standard array forming response displayed in the (t, x)- and (f, k_x)-domains (see Figures 18a and 19a). The same procedure as the 2D case was followed to quantify the noise attenuation performed by the 3D MVDR beamformer. A value of 0.0149 was obtained for error e_{fk} with the 3D MVDR beamformer, which is much less than 0.0630 obtained for the standard array. This indicates that the MVDR beamformer gives a result much closer to the desired array response compared with standard array forming.

MVDR beamformer on single-sensor field data

In this section, we consider the 2D and 3D MVDR beamformer used on single-sensor field data. These data were recorded using a strip of five lines of single sensors spaced at 5 m in the inline and crossline directions. The seismic energy was generated with dynamite, the source spacing was 20 m, and source locations were on only the central line of single sensors. One purpose of the project, whose records are used in this section, was to apply the MVDR technique and compare it with standard array forming. In this particular case, the field data were affected by variation in the amplitude and

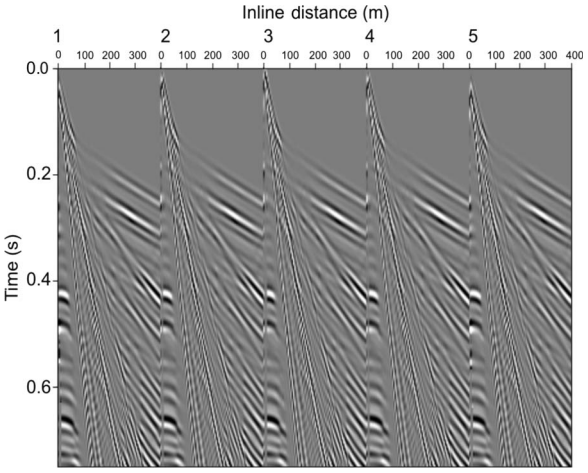

Figure 16. Synthetic record with five seismograms for 80 single-sensors with 5-m spacing (inline direction). Depth model parameters as defined in Figure 9.

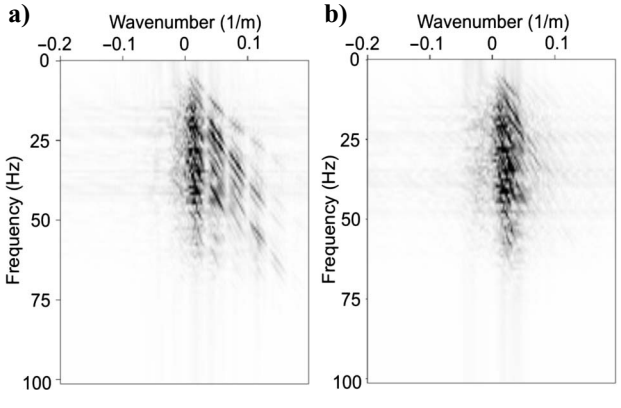

Figure 15. The (f, k_x)-amplitude spectrum of synthetic seismogram after (a) standard array forming and (b) MVDR beamforming. The same display parameters apply.

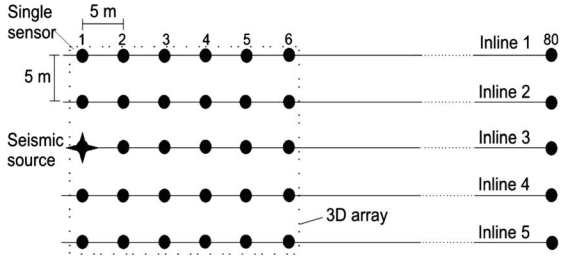

Figure 17. The 3D array with six inline and five crossline elements with the position of the seismic source.

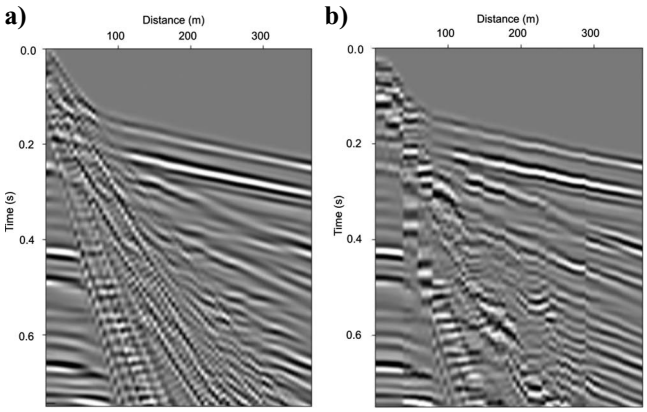

Figure 18. (a) Standard array-forming and (b) MVDR beamforming responses for arrays with 6×5 elements for finite-difference data. Depth model parameters as defined in Figure 9.

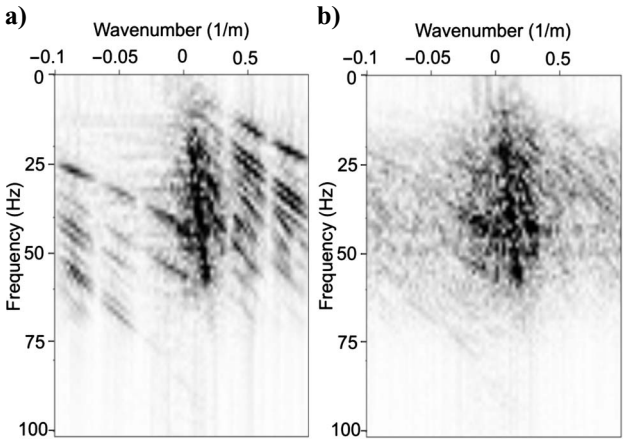

Figure 19. The (f, k_x)-amplitude spectrum of (a) standard array forming and (b) MVDR beamforming responses for arrays with 6×5 elements. The same display parameters apply.

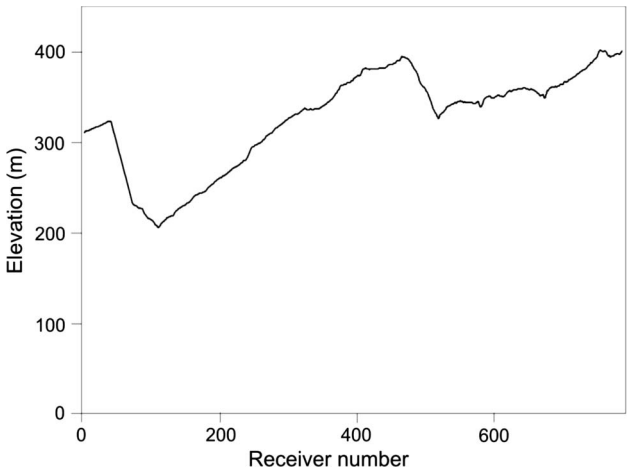

Figure 20. Elevation variations along the seismic profile of field data.

phase because data acquisition took place in a hilly area with a notable elevation difference along one receiver array (see Figure 20). In addition, lateral velocity variation is known to be present in this area, especially in shallower layers. Amplitude variation occurred because of soil conditions that locally did not provide good soil-geophone coupling.

We first applied the beamformer to a windowed record that contains 80 traces selected from a shot record obtained with single sensors placed on the third line (see Figure 21a). Looking at two time responses, we notice that remaining surface waves are easier to identify on the standard array forming response than on the MVDR beamforming response (see Figure 21b and c). We used an inline array with 12 elements. If we compare the standard array forming with the MVDR beamforming response in the (f, k_x)-domain as depicted in Figure 22, we notice clear aliased energy to be concentrated around a wavenumber of 0.05 m^{-1} and a frequency of 10 Hz on the standard array-forming response. Conversely, this aliased energy is seen to be more attenuated after MVDR beamforming (see Figure 22b and c). The parameter ε required for the computation of MVDR weights was determined using the singular value decomposition of the signal covariance matrix. This matrix was computed again using a k-filtered version of the analyzed record over the interval $(-k_{N,new}, +k_{N,new})$ obtained for the 10-m group interval. The second matrix involved in the weight computation is the data covariance matrix, $\mathbf{R_x}$, and it was computed based on raw single-sensor records. The best out-of-the-new-spatial-band energy attenuation

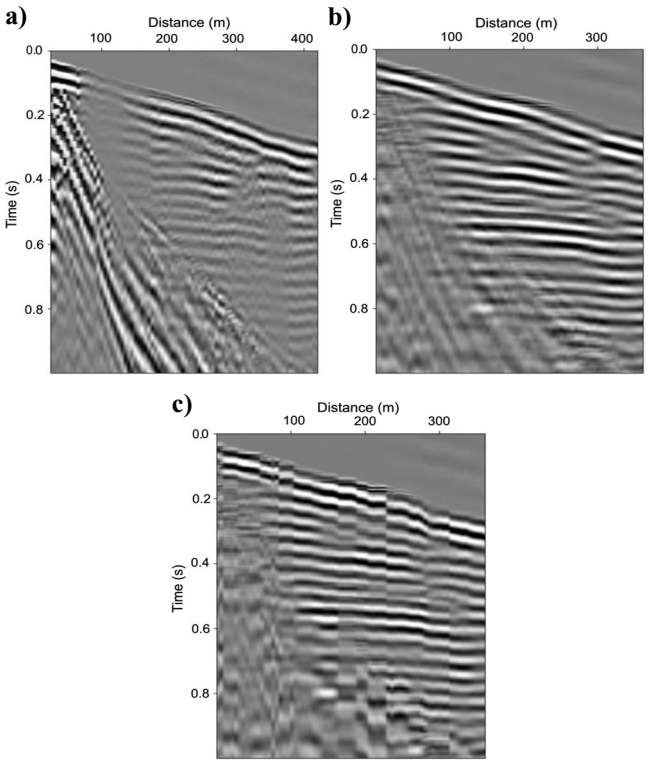

Figure 21. (a) Raw field record after (b) standard array forming and (c) MVDR beamforming displayed in the time domain.

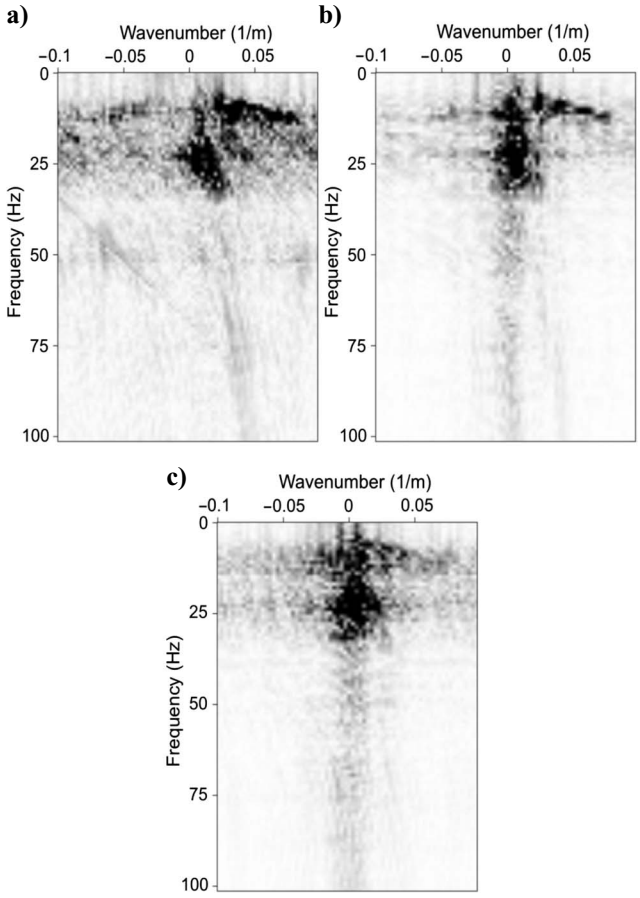

Figure 22. The (f, k_x)-amplitude spectrum of (a) raw field record after (b) standard array forming and (c) MVDR beamforming. The same display parameters apply.

obtained was for $\varepsilon = 0.02$. To quantify the effectiveness of noise attenuation performed by the 2D MVDR beamformer using equation 12, we noted $e_{fk} = 0.0088$ for the MVDR beamforming response and the higher value of $e_{fk} = 0.0118$ for the standard-array response.

In addition, the MVDR beamformer can attenuate noisy traces that do not carry seismic information. In this example, one noisy trace can appear multiplied on the standard-array response, although its presence is attenuated completely on the MVDR beamformer response (see Figure 23).

Next we considered a partial 3D shot record with the 3D MVDR beamformer (see Figure 24). In this case, we applied the MVDR algorithm for an array with 12 inline × 5 crossline elements. The standard array forming and MVDR beamforming responses are displayed in Figure 25. By comparing these two results, we notice better out-of-the-new-spatial-band energy attenuation by the MVDR algorithm. The size of the new spatial band depends on the value of the group interval, which here is 10 m. By looking at both responses displayed in the (f, k_x)-domain, we can see clearly that the standard array-forming response has a remaining surface-wave energy concentrated around a wavenumber of 0.05 m^{-1} and a frequency of

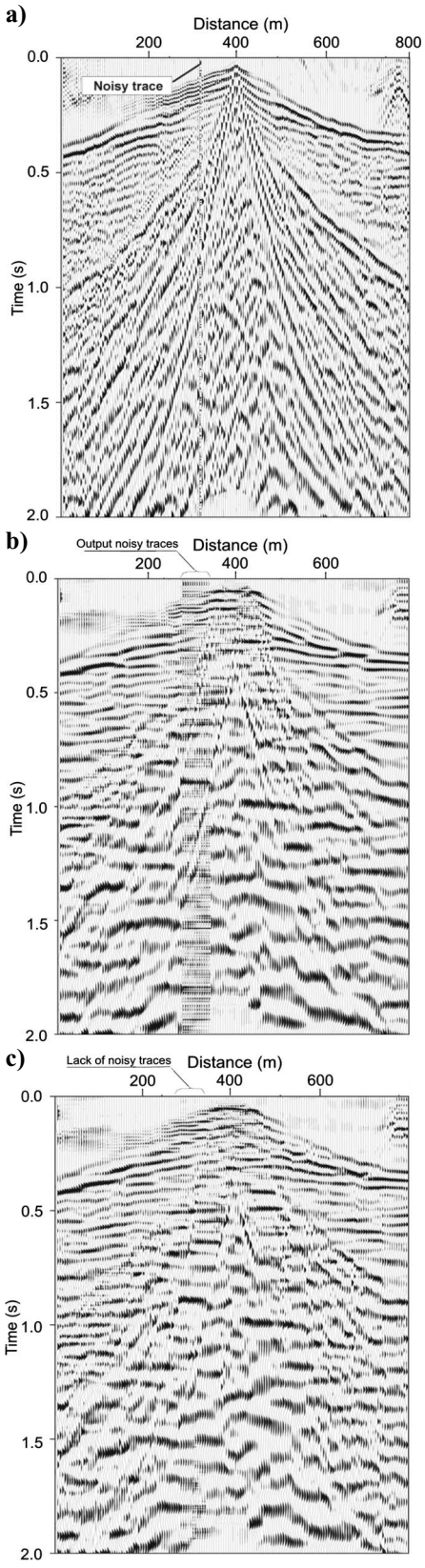

Figure 23. (a) Raw field record after (b) standard array forming and (c) MVDR beamforming.

10 Hz, whereas the MVDR beamformer is much less (see Figure 26). The error in amplitude e_{fk} shows a value of 0.0142 for the MVDR beamformer and $e_{fk} = 0.0158$ for the standard array-forming response.

The effectiveness of the noise attenuation performed by the MVDR algorithm also can be seen on stacked sections. A usual way to attenuate the noise is to stack the seismic data in the common-midpoint (CMP) domain after normal-moveout corrections. When we use a standard array to record the seismic data, the noise is attenuated first by this array and then by the CMP stacking. Thus we use two ways to increase the S/N ratio, apart from other techniques such as filtering.

So far, we have demonstrated that only on shot records does the MVDR algorithm result in better surface-wave attenuation than standard array forming. The analyzed data set contains 157 records, each representing five seismograms with 160 traces spaced at 5 m. This data set was introduced to 3D standard array forming and 3D MVDR beamforming. Results of the two approaches were further processed using the same flow to allow for comparison (see Table 1). Static corrections were applied first, using a replacement velocity of 1750 m/s for a final datum of + 450 m above sea level. Remaining surface waves were eliminated further using an *f-k* filter, *f-x* deconvolution, and a band-pass frequency filter of 20–24–64–70 Hz. The second step of array forming, namely the resampling to a new group interval of 10 m, was done next. Amplitude equalization was achieved using automatic gain control for a window of 300 ms. Top

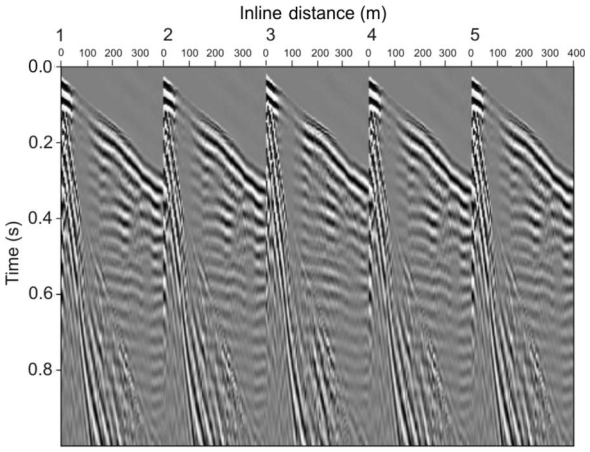

Figure 24. One record of field data.

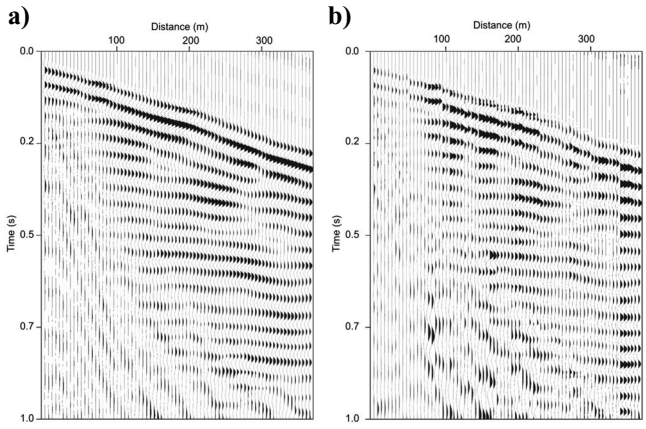

Figure 25. Field record after (a) standard array forming and (b) MVDR beamforming displayed in the time domain.

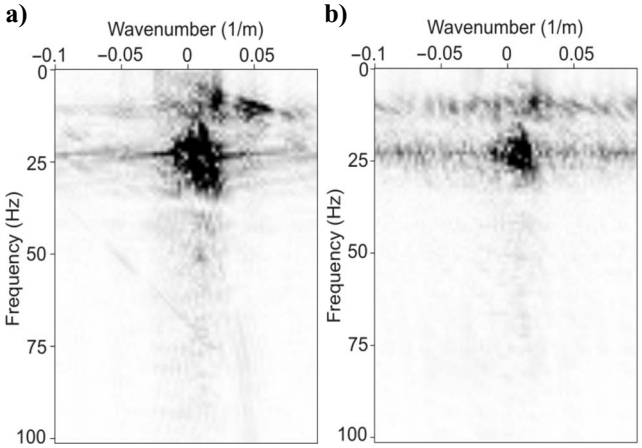

Figure 26. The (f, k_x)-amplitude spectrum of (a) standard array-forming and (b) MVDR beamforming responses. The same display parameters apply.

Table 1. Comparison of results for data set introduced to 3D standard array forming and 3D MVDR beamforming.

Processing steps	Parameters
Input seismic data	2-s trace length
	157 shots
Geometry	2D land geometry
Static corrections	Replacement velocity = 1750 m/s
	Final datum = + 450 m
Desampling in time	2 ms
Trace muting	Top (first arrivals and noise before)
Automatic gain control	300 ms
FK filter	Accept, fan polygon
Trace muting	Top (remaining noise)
Automatic gain control	300 ms
Band-pass frequency filtering	Zero-phase, frequency, 20–24–64–70 Hz; Notch filter, 50 Hz, window of 4 Hz
FX deconvolution	Wiener Levinson, 500 ms, 20–70 Hz
Automatic gain control	500 ms
Spatial resampling	Group interval of 10 m
Velocity analysis	Yes
Normal moveout corrections	Yes
Stacking	Yes

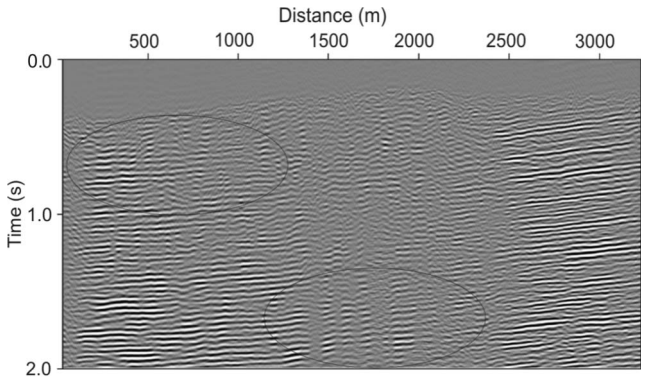

Figure 27. Time section of field data set, based on 3D MVDR beamforming.

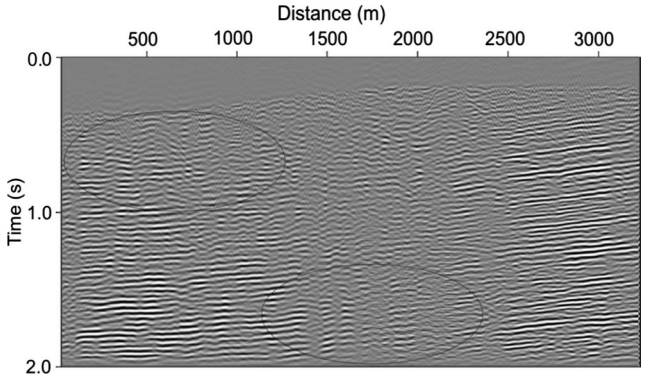

Figure 28. Time section of field data set, based on 3D standard array forming.

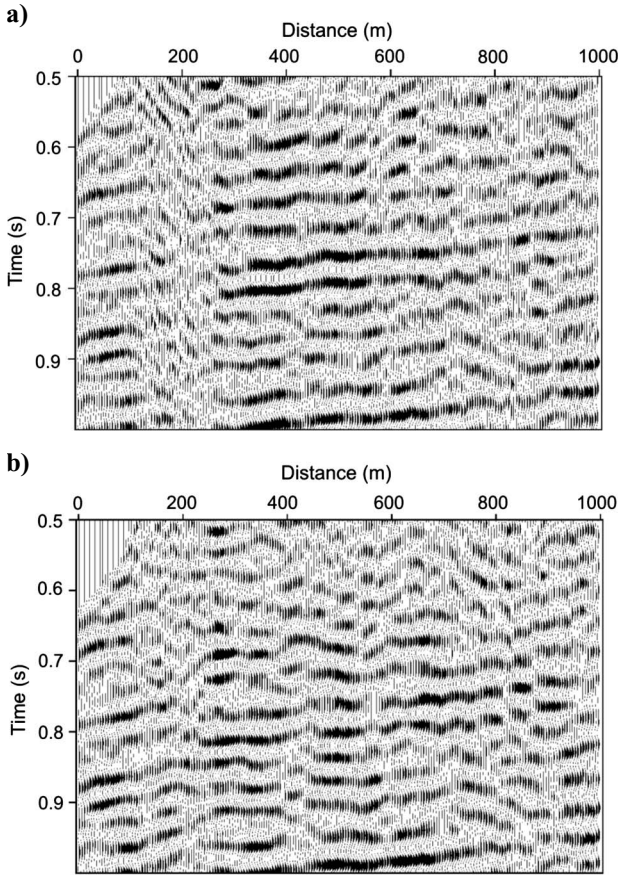

Figure 29. Windowed time sections of field data set, based on (a) 3D MVDR beamforming and (b) 3D standard array forming.

mute was applied to remove first arrivals and the advance noise. CMP stacking of seismic data used a 2D velocity model provided by the velocity analysis.

When we compare two time sections obtained in this way, we notice an improvement in the continuity of some reflectors all over the section when applying the 3D MVDR responses (see Figure 27). For example, looking on the left side of both time sections, the continuity of those reflections located between 0.5 s and 1 s is stronger. These same reflections are weaker and discontinuous with the 3D standard array-forming result (see Figure 28).

Both sides of the time sections show high reflectivity. This is caused partially by the favorable S/N ratio that characterizes recordings and partially by the 3D MVDR beamforming algorithm. The central part of the section has a very low S/N ratio because of the low quality of input data, which is a result of field conditions of rugged topography and unconsolidated soil resulting in bad geophone coupling. Use of the 3D beamformer enhanced the S/N ratio of analyzed recordings. The amplitude of some reflectors was higher after MVDR beamforming than after standard array forming. See, for example, the group of reflectors located between 1500–2000 m on the time section at the time interval of 1.6–1.9 s (see Figure 27). Some shallow reflectors also appear to be more continuous (see Figure 29a).

CONCLUSIONS

The MVDR beamformer, presented in this paper, is an algorithm adapted from similar algorithms published in the electrical engineering literature, aiming to attenuate undesired energy. In seismic exploration, this undesired energy is located outside and within the new spatial band defined by the value of the group interval. Its application on single-sensor seismic data required a different definition of the desired signal covariance, being computed using groups of traces chosen from a wavenumber-filtered single-sensor record.

Modeling results show that it can be used successfully for seismic data in combination with single-sensor recordings. Application of 2D or 3D MVDR beamforming to synthetic data showed noise attenuation appreciably better than that provided by either 2D or 3D standard array forming. Quantitative and qualitative estimations of this attenuation made by comparing responses displayed in the (t, x)- and (f, k_x)-domains support this observation. The error shows smaller values for MVDR beamforming in all cases, for synthetic and field records, which means this algorithm provides us with more acceptable responses than those obtained by alternative processing.

Application of the 3D MVDR beamformer to prestack data enhanced the signal-to-noise ratio of the stacked data more than standard array forming, including in those areas where the S/N is very low. We notice reflections are more continuous and have higher am-

plitudes in the time section based on MVDR responses. In addition, the MVDR algorithm works well with data that have a very low S/N ratio, which is encouraging because land seismic data often have this characteristic.

The effectiveness of the presented algorithm is lower regarding the attenuation of the random noise introduced by wind motion, cable vibrations, etc.

ACKNOWLEDGMENTS

The authors thank all reviewers for their helpful comments and indications that helped improve the quality of this paper. The authors thank Professor Alle-Jan van der Veen for his introduction to the theory concerning beamforming. The authors thank Shell International Exploration and Production and Professor Wim Mulder for allowing us to use the finite-difference modeling code to obtain some of the synthetic seismic records. The authors give special thanks to Dr. Giovanni Bertotti and Dr. Liviu Matenco for their support during the seismic data acquisition.

This work was sponsored by the Research Centre of Integrated Solid Earth Sciences (ISES), Netherlands.

REFERENCES

Anstey, N., 1986, Whatever happened to ground-roll? The Leading Edge, **5**, 40–46.

Bell, K. L., Y. Ephraim, and H. L. Van Trees, 2000, A Bayesian approach to robust adaptive beamforming: IEEE Transactions on Signal Processing, **48**, 386–398.

J. Capon, 1969, High resolution frequency-wavenumber spectrum analysis: Proceedings of the IEEE, **57**, 1408–1418.

Feldman, D. D., and L. J. Griffiths, 1994, A projection approach to robust adaptive beamforming: IEEE Transactions on Signal Processing, **42**, 867–876.

Godara, L. C., 1986, Error analysis of the optimal antenna array processors: IEEE Transactions on Aerospace and Electronic Systems, **22**, 395–409.

Harmanci, K., J. Tabrikian, and J. L. Crolik, 2000, Relationship between adaptive minimum variance beamformers and optimal source localization: IEEE Transactions on Signal Processing, **48**, 1–10.

Hoffe, B. H., G. F. Margrave, R. R. Stewart, D. S. Foltinek, H. C. Bland, and P. M. Manning, 2002, Analyzing the effectiveness of receiver arrays for multicomponent seismic exploration: Geophysics, **67**, 1853–1868.

Jian, L., P. Stoica, and Z. Wang, 2003, On robust Capon beamforming and diagonal loading: IEEE Transactions on Signal Processing, **51**, 1702–1715.

Johnson, D. H., and D. E. Dudgeon, 1993, Array signal processing: Concepts and techniques: Prentice-Hall, Inc.

Monzingo, R. A., and T. W. Miller, 1980, Introduction to adaptive arrays: John Wiley and Sons, Inc.

Panea, I., and G. G. Drijkoningen, 2006, Adaptive beamformers and time corrections: 68th Annual Conference and Exhibition, EAGE, Extended Abstracts, F031.

Panea, I., G. G. Drijkoningen, A. J. van der Veen, G. Bertotti, and L. Matenco, 2005, Applications of adaptive beamformers on seismic data: 67th Annual Conference and Exhibition, EAGE, Extended Abstracts, P052.

Raghunath, K. J., and V. U. Reddy, 1992, Finite data performance analysis of MVDR beamformer with and without spatial smoothing: IEEE Transactions on Signal Processing, **40**, 2726–2735.

Reed, I. S., J. D. Mallett, and L. E. Brennan, 1974, Rapid convergence rate in adaptive arrays: IEEE Transactions on Aerospace and Electronic Systems, **10**, 853–863.

Shahbazpanahi, S., A. B. Gershman, Z. Q. Luo, and K. M. Wong, 2003, Robust adaptive beamforming for general-rank signal models: IEEE Transactions on Signal Processing, **51**, 2257–2269.

Van Veen, B. D., 1991, Minimum variance beamforming with soft response constraints: IEEE Transactions on Signal Processing, **39**, 1964–1972.

Van Veen, B. D., and K. M. Buckley, 1988, Beamforming: A versatile approach to spatial filtering: IEEE ASSP, **5**, 4–24.

Vermeer, G. J. O., 1990, Seismic wavefield sampling: SEG.

Vorobyov, S. A., A. B. Gershman, and Z. Q. Luo, 2003, Robust adaptive beamforming using worst-case performance optimization: A solution to the signal mismatch problem: IEEE Transactions on Signal Processing, **51**, 313–324.

Wax, M., and Y. Anu, 1996, Performance analysis of the minimum variance beamformer in the presence of steering vector errors: IEEE Transactions Signal Processing, **44**, 938–947.

Zoltowski, M. D., 1988, On the performance of the MVDR beamformer in the presence of correlated interference: IEEE Transactions on Acoustics, Speech, and Signal Processing, **36**, 945–947.